

Magnetism manipulation in ferromagnetic/ferroelectric heterostructures by electric field induced strain

Xiaobin Guo(郭晓斌), Dong Li(李栋), Li Xi(席力)

Citation: Chin. Phys. B . 2018, 27(9): 097506. **doi:** 10.1088/1674-1056/27/9/097506

Journal homepage: http://cpb.iphy.ac.cn; http://iopscience.iop.org/cpb

What follows is a list of articles you may be interested in

First-order reversal curve investigated magnetization switching in Pd/Co/Pd wedge film

Yan Li(李岩), Wei He(何为), Rui Sun(孙瑞), Zi-Zhao Gong(弓子召), Na Li(李娜), Qeemat Gul, Xiang-Qun Zhang(张向群), Zhao-Hua Cheng(成昭华)

Chin. Phys. B . 2018, 27(4): 047503. **doi:** 10.1088/1674-1056/27/4/047503

NMR evidence of charge fluctuations in multiferroic $CuBr_2$

Rui-Qi Wang(王瑞琦), Jia-Cheng Zheng(郑家成), Tao Chen(陈涛), Peng-Shuai Wang(王朋帅), Jin-Shan Zhang(张金珊), Yi Cui(崔祎), Chong Wang(王冲), Yuan Li(李源), Sheng Xu(徐胜), Feng Yuan(袁峰), Wei-Qiang Yu(于伟强)

Chin. Phys. B . 2018, 27(3): 037502. **doi:** 10.1088/1674-1056/27/3/037502

Control of spins in a nano-sized magnet using electric-current

Hong-yu Wen(文宏玉), Jian-bai Xia(夏建白)

Chin. Phys. B . 2017, 26(4): 047501. **doi:** 10.1088/1674-1056/26/4/047501

Lumped modeling with circuit elements for nonreciprocal magnetoelectric tunable band-pass filter

Xiao-Hong Li(李小红), Hao-Miao Zhou(周浩淼), Qiu-shi Zhang(张秋实), Wen-Wen Hu(胡文文)

Chin. Phys. B . 2016, 25(11): 117505. **doi:** 10.1088/1674-1056/25/11/117505

Magnetoelectric memory effect in the Y-type hexaferrite $BaSrZnMgFe_{12}O_{22}$

Fen Wang(王芬), Shi-Peng Shen(申世鹏), Young Sun(孙阳)

Chin. Phys. B . 2016, 25(8): 087503. **doi:** 10.1088/1674-1056/25/8/087503

TOPICAL REVIEW — Spin manipulation in solids

Magnetism manipulation in ferromagnetic/ferroelectric heterostructures by electric field induced strain*

Xiaobin Guo(郭晓斌), Dong Li(李栋), and Li Xi(席力)†

Key Laboratory for Magnetism and Magnetic Materials of Ministry of Education, School of Physical Science and Technology, Lanzhou University, Lanzhou 730000, *China*

(Received 27 April 2018; revised manuscript received 9 June 2018; published online 28 August 2018)

Magnetization manipulation by an electric field (E-field) in ferromagnetic/ferroelectric heterostructures has attracted increasing attention because of the potential applications in novel magnetoelectric devices and spintronic devices, due to the ultra-low power consumption of the process. In this review, we summarize the recent progress in E-field controlled magnetism in ferromagnetic/ferroelectric heterostructures with an emphasis on strain-mediated converse magnetoelectric coupling. Firstly, we briefly review the history, the underlying theory of the magnetoelectric coupling mechanism, and the current status of research. Secondly, we illustrate the competitive energy relationship and volatile magnetization switching under an E-field. We then discuss E-field modified ferroelastic domain states and recent progress in non-volatile manipulation of magnetic properties. Finally, we present the pure E-field controlled 180° in-plane magnetization reversal and both E-field and current modified 180° perpendicular magnetization reversal.

Keywords: electric field, volatile and non-volatile, magnetization switching

PACS: 75.85.+t, 77.55.Nv, 77.80.bn **DOI:** 10.1088/1674-1056/27/9/097506

1. Introduction

Magnetic tunnel junctions (MTJs) with an AlO_x or MgO insulating barrier have been widely used in many fields, such as the read heads of hard disk drives (HDD), weak magnetic field detection, and sensitive magnetometers.[1–4] The essence of MTJs is the identification of parallel and antiparallel magnetization of two ferromagnetic electrodes, with low-resistance and high-resistance states, respectively. This has been regarded as an outstanding example of the commercialization of scientific research.[5] At present, in both the cases of traditional HDD and the developing magnetic random access memory (MRAM), the question of writing magnetic information to represent "0" and "1", i.e., the manipulation of the two distinguishable magnetization states in MTJs, is still a challenging issue with respect to an in-depth understanding of the physical mechanism involved and the realization of practical applications. In a traditional magnetic field based MRAM, the magnetization orientation of the free layer in the MTJs is controlled by magnetic fields produced by two orthogonal conducting lines. The approach is hindered by several technical bottlenecks, which include:[5,6] (i) the conducting lines occupy a significant amount of space and the broad magnetic field distribution could disturb the adjacent memory cell; and (ii) when the size of memory cells is decreased further to improve storage density, a high current density ($\sim 10^7$ A/cm^2) is required. In recent years, based on the spin transfer torque (STT) effect[7–9] and spin–orbit torque (SOT) effect,[10–12] STT-MARM has entered a stage of industrialization,[13] and the SOT-MRAM has been realized in the laboratory.[14] However, they also face some technical difficulties, such as how to decrease the threshold current density (J_c) to about 10^5 A/cm^2 and realize magnetization switching without the assistance of an in-plane magnetic field in SOT-MRAM.[15] In addition to the magnetic field and current induced relevant effects, light, strain, phase transition, and electric field (E-field) are also able to effectively regulate magnetism.[16–19] Among them, E-field control of magnetic properties not only is able to significantly decrease the Joule heating effect, but also can realize non-volatile, reversible, and high-density data storage with low power consumption.

Generally, in the area of E-field control of magnetism, candidate materials primarily include magnetic semiconductors,[20] ferromagnetic metals,[21] and multiferroic materials.[22] The propagation of domain walls (DWs) and the modification of magnetic properties are promising approaches for the realization of high-density magnetic memory and magnetic logic elements. Lei *et al.* demonstrated that DW motion can be electrically controlled through strain-mediated magnetoelectric coupling in piezoelectric/ferromagnetic nanostructures at room temperature, and that the energy barrier for DW motion can be doubled under reasonable electric fields.[23] Rushforth *et al.* demonstrated that voltage induced strain can

*Project supported by the National Natural Science Foundation of China (Grant No. 51671098) and the Program for Changjiang Scholars and Innovative Research Team in University, China (Grant No. IRT16R35).

†Corresponding author. E-mail: xili@lzu.edu.cn

© 2018 Chinese Physical Society and IOP Publishing Ltd

effectively regulate magnetic anisotropy, anisotropic magnetoresistance, and nonvolatile switching of the magnetization direction in a (Ga,Mn)As device bonded to a piezoelectric transducer. Meanwhile, calculations based on the mean-field kinetic exchange model of (Ga,Mn)As facilitate a microscopic understanding of the measured effect.[24] Li *et al.* reported that the piezo voltages manipulate the magnetic properties of the Fe/n-GaAs/piezoelectric heterostructure. By measuring the magnetic hysteresis loops under the piezo voltages, the manipulation of two-jump to one jump magnetization switching can be realized. These findings could be very important for future metal-semiconductor spintronic applications.[25] In comparison, many investigations have focused on multiferroic materials combined with ferroelectricity, ferromagnetism, and ferroelasticity. The three ferroic order interactions can lead to diverse phenomena. For example, the ferroelectricity and ferroelasticity present the piezoelectric effect, ferromagnetism and ferroelasticity present the piezomagnetic effect, and ferroelectricity and ferromagnetism present the magnetoelectric (ME) effect. Magnetism could be manipulated by the converse ME coupling effect with an applied E-field, which is a promising method to fabricate energy-efficiency spintronic devices.[26–28] Single-phase multiferroic materials are rare and only present ME coupling effects well below room temperature.[29] $BiFeO_3$ is a unique example of such a material that has already been proved to exhibit ferroelectricity and weak anti-ferromagnetism (AFM) at room temperature.[30] For artificial ferromagnetic/ferroelectric (FM/FE) heterostructures with coupling between the ferromagnetic layer with a high magnetostrictive effect and a ferroelectric layer with a large piezoelectric effect, the magnetic properties of the FM can be effectively adjusted by the converse ME coupling effect. The coupling mechanisms in such FM/FE heterostructures mainly include the charge mediated effect through charge accumulation/dissipation at the FM/FE interface, the exchange bias mediated effect resulting from the AFM properties of the FE layer, the strain mediated effect by means of transferring strain from the FE layer to the FM layer, as well as the emergent mechanisms of orbital reconstruction and the electrochemical effect in ultrathin films. It should be noted that the aforementioned coupling mechanisms may coexist, and the main features of the last one are highlighted in previous reviews.[27,31] Among them, the strain-mediated mechanism has received a lot of attention in recent years, because this method is particularly convenient and effective at room temperature. Moreover, the incorporation of FE materials is optional for this purpose, given the large piezoelectric coefficients and/or the piezoelectric memory effect. For example, $BaTiO_3$,[32] $Pb(Zr_{1-x}Ti_x)O_3$ (PZT),[33] $[Pb(Mg_{1/3}Nb_{2/3})O_3]_x$-$[PbTiO_3]_{1-x}$ (PMN-PT),[34] and $[Pb(Zn_{1/3}Nb_{2/3})O_3]_x$-$[PbTiO_3]_{1-x}$ (PZN-PT)[35] are usually used as FE layers in the FM/FE heterostructures. Alternative materials which exhibit magnetostriction effects that serve as FM layers can be widely chosen from the amorphous to single crystal phase, and from the magnetic isotropic to the magnetic anisotropic materials. So far, E-field induced strain-mediated orientation of magnetization, magnetic anisotropy, coercivity, and ferromagnetic resonance frequency have been realized in ferromagnetic/piezoelectric actuator hybrid structures or FM/FE heterostructures.[36–40]

In this context, we will review some exciting research on E-field control of magnetism by means of strain-mediated magnetoelectric coupling. In Section 2, we will examine the volatile magnetization switching of magnetic thin films with in-plane isotropic or uniaxial magnetic anisotropy (UMA). In particular, the impact of E-field induced additional UMA on the magnetic anisotropy competitive relationship is described. In Section 3, the non-volatile magnetization manipulation in FM/PMN-PT with ferroelectric domain switching is presented. Based on the epitaxial FM film on a single crystal FE substrate, we introduce E-field controlled non-volatile and reversible magnetization switching in epitaxial FM/PMN-PT heterostructures. In Section 4, we discuss 180° magnetization switching based on the pure E-field method and the combination of the E-field and current effects for FM films with in-plane magnetic anisotropy and perpendicular magnetic anisotropy (PMA), respectively.

2. Volatile magnetization switching

Compared to the interface charge mediated effect, transferring the strain from FE to FM film usually leads to giant magnetic property modification in thick FM films. In normal (001) PMN-PT materials,[41] the E-field dependence on the in-plane strain (S–E) curve shows symmetric butterfly-like variation. After removing the applied E-field, the residual stress vanishes, i.e., the in-plane strain is volatile. When an isotropic magnetic films is fabricated on the (001) PMN-PT substrate, its volatile magnetic response shows a similar behavior to the S–E curve. In $CoFe_2O_4$/(001) PMN-PT heterostructure,[42] as shown in Figs. 1(a) and 1(b), the in-plane and out-of-plane relative changes in the magnetization $[\Delta M/M(0)]$ as a function of the E-field present an opposite butterfly shape with a maximum in-plane $\Delta M/M(0)$ of approximately 6%, and the magnetization returns to its initial state when the E-field is switched off. Volatile magnetization manipulation was also reported in $La_{0.7}Sr_{0.3}MnO_3$/(001)PMN-PT[43] and $Co_{40}Fe_{40}B_{20}$/(011)PMN-PT[44] heterostructures with the maximum change of the in-plane $\Delta M/M(0)$ reaching 25% and 83%, respectively. Notably, a reversible 90° magnetic easy

axis (EA) rotation was simultaneously observed for the applied E-field.

For the amorphous or polycrystalline FM films with UMA, the hysteresis loop (M–H) along the EA direction is square, whereas the hysteresis loop along the hard axis (HA) direction is slanted with a fairly small remanence ratio (M_r/M_s). In such FM/FE heterostructures, the total free energy can be written as the sum of the UMA and the additional magnetoelastic energy, assuming that the strain induced UMA is along the original HA direction. This can be represented expressed as follows:

$$F = \frac{V[-\mu_0 M_s H_K \sin^2(\phi) - 3\lambda_s \sigma \cos^2(\phi)]}{2}, \qquad (1)$$

where V is the volume of the FM film, M_s is the saturation magnetization, H_K is the effective UMA field, λ_s is the saturation magnetostriction, σ is the mechanical stress, and φ is the angle between the magnetization and HA. The angular dependence of the free energy can be presented as shown in Fig. 2(a). The magnetic EA is always along the direction in which the free energy is a minimum. From Fig. 2(a), it can be seen that EA is along the 90° and 270° direction without applying any strain. When a compress strain is applied, i.e., negative stress, the original magnetic EA remains. When applying a positive stress, the energy value at all angles is constant, i.e., isotropic magnetic properties can be observed. Once the positive stress is further increased, the minimum free energy direction appears at 0° and 180°, indicating a feasible 90° magnetic EA rotation.[45]

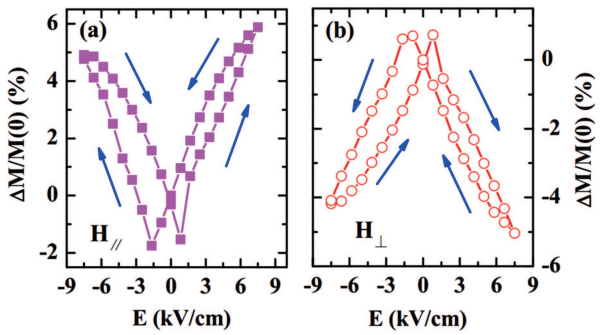


Fig. 1. (color online) (a) In-plane $\Delta M/M(0)$–E loop, the magnetic field is 0.05 T. (b) Out-of-plane.$\Delta M/M(0)$–E loop, the magnetic field is 0.2 T (from Fig. 4 in Ref. [42]).

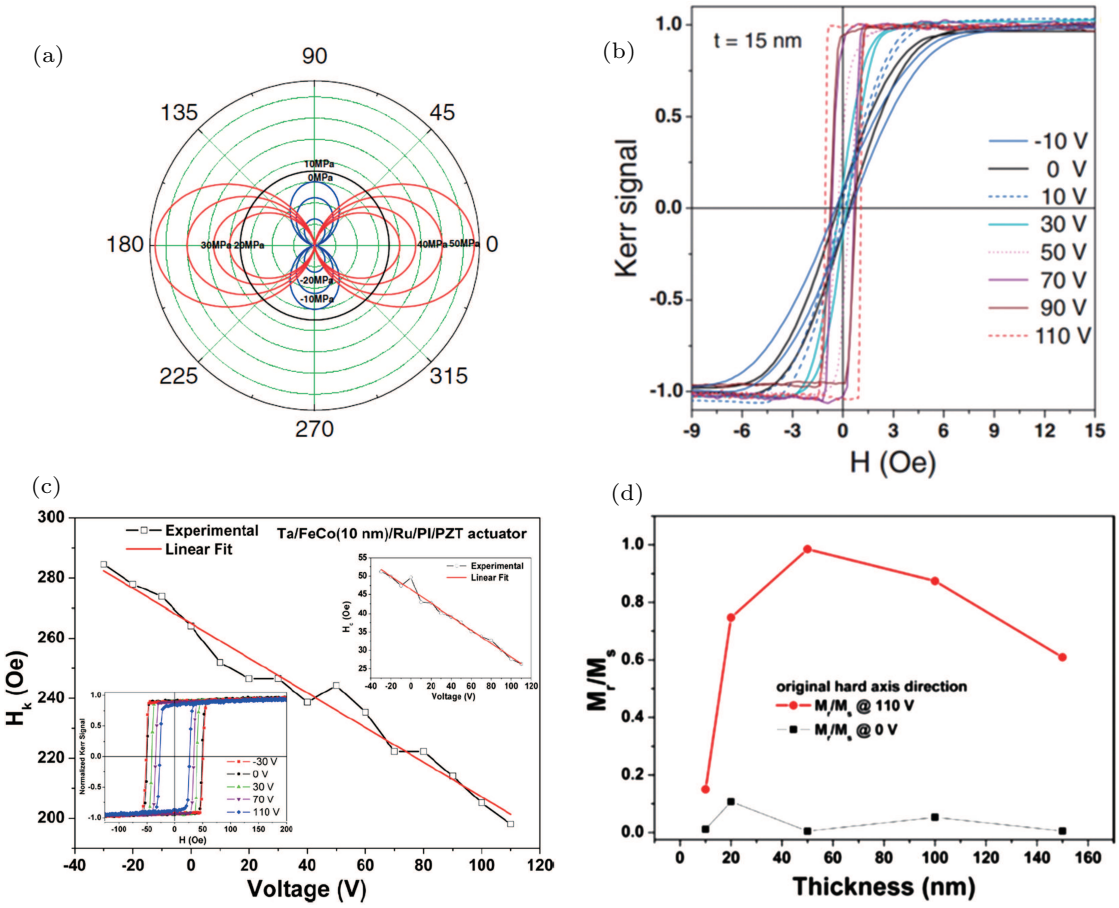


Fig. 2. (color online) (a) Theoretical calculation of the angular dependence of the free energy for different applied stresses parallel to the initial hard axis of the FeNi film according to Eq. (1). In this polar pattern, the energy decreases from the inner circle to the outer circle (from Fig. 2 in Ref. [45]). (b) M–H loops of FeNi (15 nm)/piezoelectric actuator for different applied voltages (from Fig. 3(c) in Ref. [45]). (c) Voltage dependence of the H_K of FeCo (10 nm)/PI heterostructures. The left and right insets show the M–H loops and the coercivity along the original EA direction at different applied voltages (from Fig. 4 in Ref. [47]). (d) Thickness-dependent remanence ratios at 0 and 110 V of the piezoelectric actuators along the original hard axis directions (from Fig. 6 in Ref. [47]).

A piezoelectric actuator can be used to produce directional stress that is proportional to the applied voltage. Positive and negative voltages could induce tensile and compressive stress, respectively.[46] By applying strain along the initial HA direction of the FM films, Xi *et al.* reported a 90° shift of the magnetization in 15 nm thick FeNi/glass film under the application of a voltage of 110 V by magneto-optical Kerr effect measurements (Fig. 2(b)). The film-thickness dependence of the EA rotation angle was explained by the thickness dependent magnetostriction of FeNi films.[45] In order to avoid the clamping effect between the substrate and piezoelectric actuator as well as to further improve the strain transmission efficiency, flexible polyamides (PI) were used to replace the glass substrate. In FeCo/PI/piezoelectric actuator heterostructures, a 90° rotation of the UMA was achieved in 50 nm thick FeCo films under a voltage of 70 V. Figures 2(c) and 2(d) show the voltage dependence of the UMA field and the coercivity for a 10 nm thick FeCo film, as well as M_r/M_s against thickness for 110 V and 0 V with the values obtained by measuring the *M*–*H* curves at corresponding conditions.[47] Since the piezoelectric actuator produced strain exhibits linear variation under an applied *E*-field, the magnetism modification at different voltages is also volatile.

3. Non-volatile magnetism manipulation

In the volatile FM/FE heterostructures, the changed magnetic state will return to the original state once the applied *E*-field is removed. Obviously, volatile magnetism manipulation cannot meet the requirements of magnetic information storage.[31,48,49] Thus, non-volatile magnetism manipulation by the *E*-field in FM/FE heterostructures has attracted intensive attention due to the significant scientific value of the procedure and the technological breakthrough of novel ME devices. Despite the non-volatile magnetization reversal in ultrathin FM films based on the charge-mediated mechanism, strain-mediated non-volatile magnetization and magnetic anisotropy modifications were also reported in FM/FE heterostructures. Among these literatures, the (001) and (011) oriented single crystalline PMN-PT or PZN-PT with their excellent piezoelectric effects are the widely used FE substrates due to their in-plane residual stress induced by the unique ferroelectric domain switching.

3.1. *E*-field controlled magnetism in FM/(011) PMN-PT heterostructures

In 2011, Wu *et al.* reported on unipolar poling *E*-field controlled reversal and permanent magnetization reorientation in Ni/(011) PMN-PT heterostructures[50] and studied the piezoelectric strain response in (011) PMN-PT single crystals.[51] Due to the non-180° ferroelectric polarization switching from the out-of-plane to in-plane direction under a critical *E*-field (or near the coercive *E*-field), the strain state will not change after reduction of the critical *E*-field to zero, and the strain shows noticeable changes until the converse *E*-field is large enough. Thus, two stable and reversible remanent strain states are observed as represented by points E and C in the inset of Fig. 3(a). When the strain is transferred to the in-plane magnetic isotropic Ni film, it causes an obvious magnetic remanence change of approximately 50% and a magnetic anisotropy field at approximately 300 Oe in the *M*–*H* loops (Fig. 3(a)). Moreover, in FeCo/Ru/(011) PMN-PT,[52] the initial magnetic EA (HA) of the FeCo films is along the [100] ([01-1]) direction of the (011) PMN-PT substrate. After applying an *E*-field of 4 kV/cm, the magnetic EA (HA) is along the [01-1] ([100]) direction. Interestingly, the UMA occurs at a 90° rotation, and the magnetic anisotropy variation is non-volatile (Fig. 3(b)). Considering the FeCo films with two reversible and stable UMA states under ±2 kV/cm, a determinate high (low) resistance state occurs and is maintained after removal of the −2 kV/cm (2 kV/cm) *E*-field. This indicates that the data bits cells were demonstrated in FeCo/Ru/(011)PMN-PT heterostructures. Furthermore, the *E*-field induced non-volatile strain response of the (011) PMN-PT substrate was also used to control the dynamic magnetic properties of FM films. In FeCoB/(011) PMN-PT heterostructures with an amorphous state of FeCoB,[53] a strong tensile strain is generated along the in-plane [0-11] direction of (011) PMN-PT and results in a non-volatile ferromagnetic resonance (FMR) frequency change of 2.3 GHz in FeCoB film when the *E*-field changes from −6 kV/cm to 1.5 kV/cm. Figure 3(c) shows the reversible and non-volatile FMR frequency manipulation for a pulse *E*-field. In addition to the aforementioned observation, it can be seen that the −6 kV/cm and 1.4 kV/cm pulsed *E*-fields can also give rise to an FMR frequency variation of approximately 1.5 GHz. This provides a framework for realizing non-volatile, reversible, and energy efficient magnetic microwave devices. At the same time, the ferroelastic domain switching process is also analyzed by reciprocal space mapping (RSM) in (011) PMN-PT and PZN-PT.[49,53] Liu *et al.* summarized the ferroelastic domain switching of the (011) PZN-PT. When the applied *E*-field varies from the negative saturated *E*-field to the positive coercive *E*-field along the [011] direction, the ferroelectric domain switches from the out-of-plane direction to in-plane direction. In this process, only the 71° ferroelectric switching makes a contribution to a strong lattice strain along the [011] and [100] directions (Fig. 3(d)), and the 71° ferroelastic switching takes place in 80% of the entire poled area of (011) PZN-PT. The ferroelectric domain switching can completely explain the expected giant and non-volatile switching mechanism in FeCoB/(011) PZN-PT.[49]

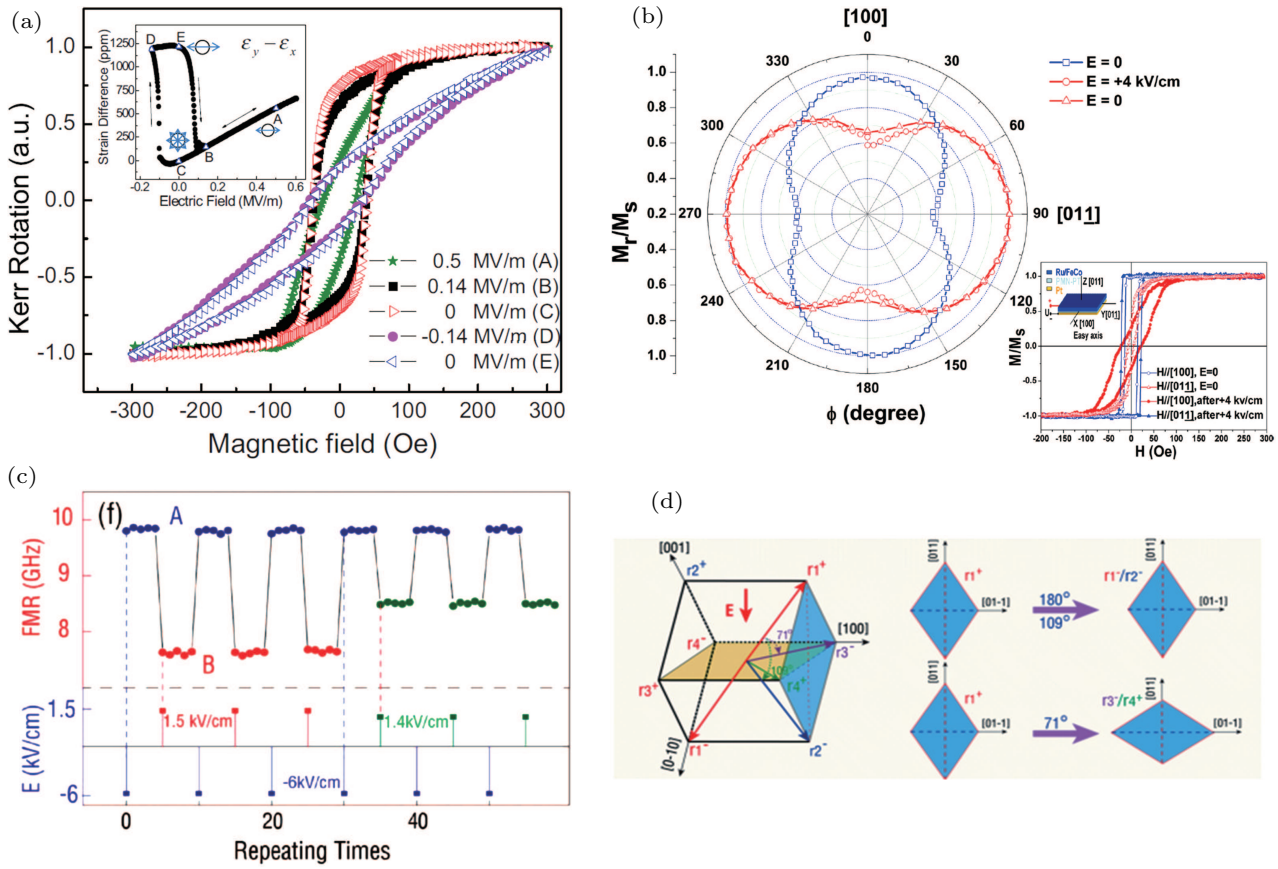


Fig. 3. (color online) (a) Normalized Kerr rotation hysteresis curves along the $\bar{y}$-direction under different E-fields. The inset shows the in-plane strain difference ($\varepsilon_y - \varepsilon_x$) as a function of the E-fields (from Fig. 3 in Ref. [50]). (b) Angular dependence of M_r/M_s with $E = 0$ (open square), 4 kV/cm (open circle), and after releasing 4 kV/cm (open triangle) E-fields. The inset gives the M–H loops without the E-field and after releasing 4 kV/cm E-fields (from Fig. 2 in Ref. [52]). (c) Voltage-impulse-induced non-volatile switching of FMR frequency in FeCoB/(011) PMN-PT heterostructures (from Fig. 1(f) in Ref. [53]). (d) Schematics of the E-field-induced ferroelectric/ferroelastic domain switching pathways in (011) oriented PZN-PT single crystal substrates (from Fig. S1(b) in Ref. [49]).

3.2. *E*-field controlled magnetism in FM/(001) PMN-PT heterostructures

In 2012, Zhang *et al.* first reported on loop-like and non-volatile magnetization manipulation in amorphous CoFeB/(001) PMN-PT by a bipolar poling E-field.[54] Figure 4(a) shows the reversible and remarkably high/low magnetization states along the [110] direction for a ± 8 kV/cm E-field pulse. Since the thickness of CoFeB is 20 nm, the interface charge-mediated effect is ignored. Based on the RSM measurement under different E-fields, they found that a 25% relative change of the magnetization switching can be attributed to the 26% change of the 109° ferroelastic domain switching in (001) PMN-PT. The loop-like converse ME response is totally different from the volatile E-field controlled magnetism in previous FM/(001)PMN-PT or PZN-PT.[42,43,55,56]

In order to determine the underlying mechanism of the distinct modification behaviors, Yang *et al.* studied the strain response of the special type of (001) PMN-PT under continuous and pulsed E-field modes. This resulted in an asymmetric butterfly-like strain–electric (S–E) curve (Fig. 4(b)) for a continuous E-field and a bipolar loop-like S–E curve for a pulsed E-field.[41] Interestingly, the butterfly-like S–E curve is composed of symmetric butterfly-like and loop-like components, and the RSM measurement shows approximately a 20% change of the 109° ferroelastic domain switching. On the contrary, in the normal (001) PMN-PT with the same nominal composition, the S–E curve is symmetric and volatile. The RSM indicates the absence of the 109° ferroelectric domain switching under an applied E-field, accompanied by volatile magnetization modification. It should be mentioned that whether the (001) PMN-PT exists or not, the aforementioned 109° ferroelectric domain switching may be related to defects during the crystal growth. The above ferroelectric properties of PZN-PT are similar to those of PMN-PT. Figure 4(c) shows the schematics of the ferroelastic domain switching pathways in (001) PZN-PT. When the E-field is along the [001] direction, only 109° polarization switching leads to a strong lattice strain along the diagonal direction in the (001) plane. This leads to a non-volatile tuning of the magnetic properties in the mechanically-coupled magnetic films deposited onto the (001) PZN-PT substrate. In FeCoB/(001) PZN-PT heterostructures, a non-volatile and reversible FMR field of 64 Oe is obtained under alternatively pulsed E-fields of 8 kV/cm and -6 kV/cm.[49]

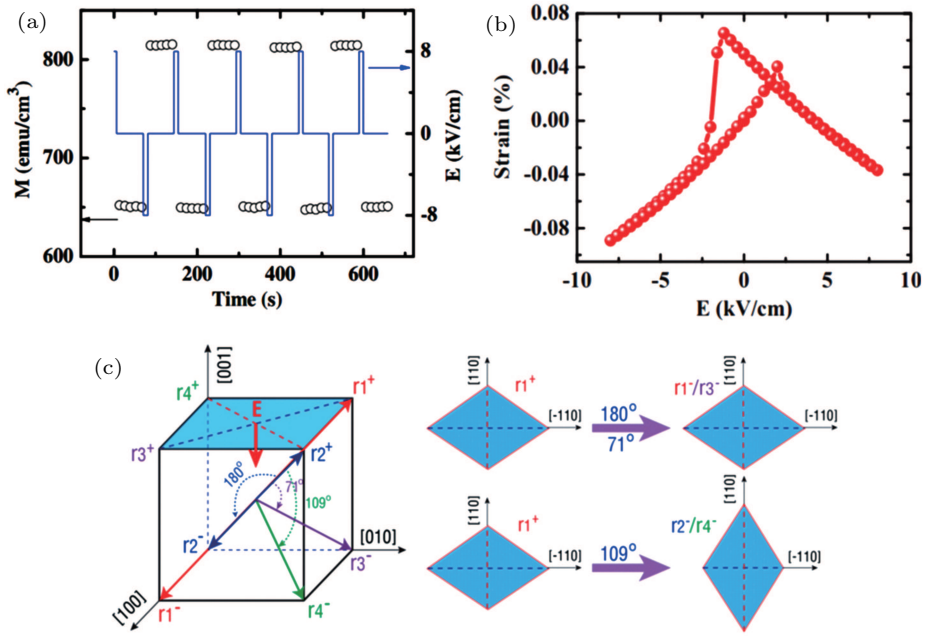


Fig. 4. (color online) (a) Repeatable high/low magnetization states (open circle) switched by pulsed E-fields (blue line) in CoFeB/(001)PMN-PT (from Fig. 1(d) in Ref. [54]). (b) S–E curves along the [110] direction of (001) PMN-PT measured by continuous measurement (from Fig. 2(a) in Ref. [41]). (c) Schematics of the E-field-induced ferroelectric/ferroelastic domain switching pathways in (011) oriented PZN-PT single crystal substrates (from Fig. S1(a) in Ref. [49]).

3.3. Magnetism manipulation in epitaxial FM/PMN-PT heterostructures

Epitaxial ferromagnetic film exhibits magnetocrystalline anisotropy, which originates from the spin–orbit coupling and correlates with the symmetry of the lattice structure. Compared to amorphous magnetic films with uniaxial magnetic anisotropy, iron-based epitaxial ferromagnetic films present biaxial magnetic anisotropy and the unique magnetization switching processes under magnetic fields.[57] Furthermore, FM films with cubic magnetocrystalline anisotropy (CMA) provide a pathway to realize multi-states magnetic information storage as long as one can precisely control the magnetization switching among the magnetocrystalline anisotropy determined energy minimum positions. Supposing a strain induced additional magnetic anisotropy is added to the film with CMA, the magnetic free energy without the external magnetic field is calculated. The simulated curves under different strain induced UMA clearly demonstrate that the magnetic easy axis rotates 90° from the initial direction (Fig. 5).[58]

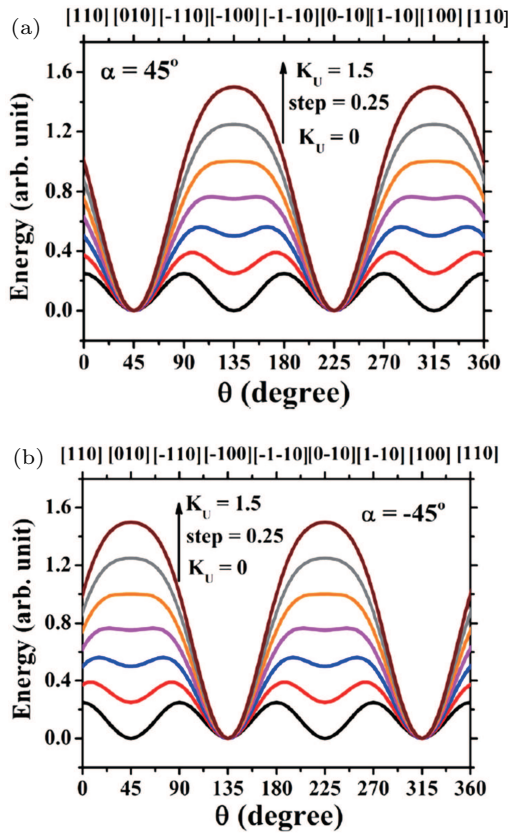


Fig. 5. (color online) Theoretical calculations on the angular dependence of the free energy for strain-induced UMA energy along [010] (a) and [100] (b) directions (from Figs. 2(c) and 2(d) in Ref. [58]).

Parkes *et al.* reported on a 90° non-volatile magnetization switching in epitaxial (001)FeGa/(001)GaAs/piezoelectric transducer heterostructures through transducer transferred strain when a voltage is applied.[59] In epitaxial (001)FeSi/(001)PMN-PT heterostructures with epitaxial relationships of FeSi(001)[100]//PMN-PT(001)[110], the magnetic anisotropy transition from four-fold CMA dominated to two-fold UMA dominated can occur subsequent to the application of negative E-fields in $Fe_{86}Si_{14}$/(001)PMN-0.32PT heterostructures. Unfortunately, the magnetic anisotropy transition is non-volatile and irreversible.[60] After modifying the composition of the ferromagnetic layer and the ferroelectric substrate, the angular dependence of the remanence (ARM) curves changes rapidly from the original four-fold to two-fold symmetries under E-fields in epitaxial $Fe_{80}Si_{20}$/(001)PMN-

0.3PT. Moreover, the non-volatile and reversible 90° magnetization switching with the dominated UMA under ±6 kV/cm is also observed. By measuring the micro-areas with a focused magneto-optical Kerr magnetometer under an *E*-field, the internal competitive relationship between the CMA energy and the UMA energy is confirmed by changing the shape of the *M*–*H* loop, as shown in Figs. 6(a) and 6(b). It illustrates that the strain-induced UMA overcomes the original HA barrier of the CMA of epitaxial $Fe_{80}Si_{20}$ films and switches the magnetization direction with MEA switching to the [010] ([100]) direction after the application of a −6 kV/cm (+6 kV/cm) pulse.[58] In Co_2FeAl/GaAs/PZT heterostructures, the strain induced planar Hall voltage of Co_2FeAl films can also be regulated by applied voltages. Moreover, based on the one and double piezo voltages control of the planar Hall effect, the logic operation architectures of NOT and NOR logic gates were proposed and demonstrated at room temperature without additional magnetic fields.[61,62]

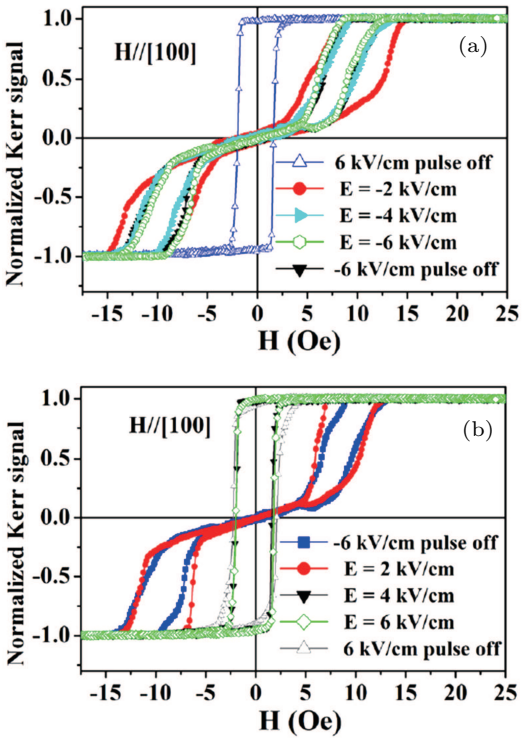


Fig. 6. (color online) Normalized Kerr *M*–*H* loops along [100] direction under negative (a) and positive (b) *E*-fields in $Fe_{80}Si_{20}$/(001)PMN-0.3PT (from Figs. 4(a) and 4(b) in Ref. [58]).

In $Fe_{86}Si_{14}$/(001)PMN-0.32PT and $Fe_{80}Si_{20}$/(001)PMN-0.3PT heterostructures, a feasible method for recovering the original CMA state is to anneal the heterostructures at a temperature of 150 °C.[58,60] However, in the epitaxial $Fe_{80}Si_{20}$/(011)PMN-0.3PT heterostructure at 300 °C post annealing, the release of interface strain leads to the reorientation of the dominated CMA when the *E*-field changes from −2.5 kV/cm to 8 kV/cm or from 2.5 kV/cm to −8 kV/cm. Conversely, when the *E*-field changes from 8 kV/cm to −2.5 kV/cm or from −8 kV/cm to 2.5 kV/cm, the two-fold dominated UMA changes back to four-fold CMA. Both kinds of magnetic anisotropies transitions are non-volatile and reversible (Fig. 7(a)). Combined with *E*-field induced 90° magnetization switching and the auxiliary magnetic field, this demonstrates that non-volatile 180° magnetization switching is accompanied by two successive 90° magnetization reversal processes (Fig. 7(b)).[63]

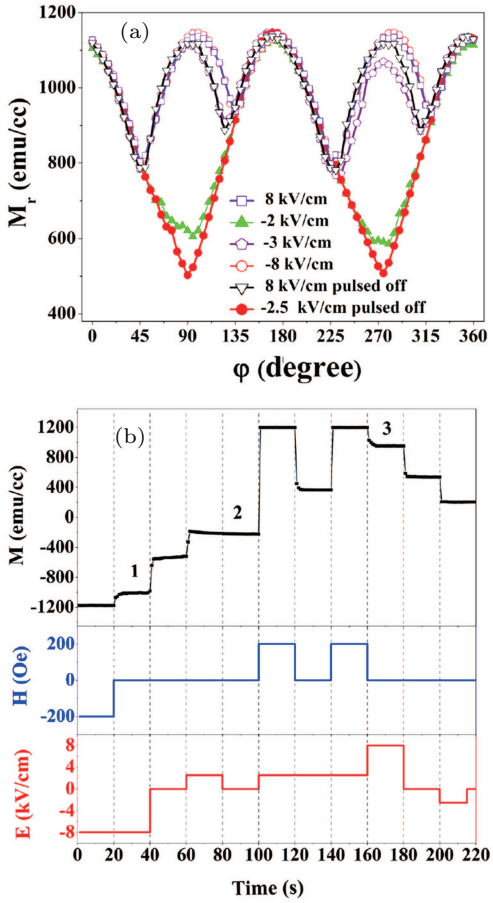


Fig. 7. (color online) (a) ARM curves with a continuously changing *E*-field as well as a pulsed *E*-field (from Fig. 3(a) in Ref. [63]). (b) *E*-field-induced magnetization variation with the assistance of a magnetic field (from Fig. 4(a) in Ref. [63]).

4. 180° magnetization switching with *E*-field

In MTJs, the parallel/anti-parallel magnetization of two ferromagnetic electrodes gives rise to distinguishable low/high resistance states. However, manipulating full 180° magnetization reversal of the free layer without external magnetic fields is a challenge in MRAM design with the low-power requirements. Given the rapid development of *E*-field control 90° magnetization reversal, intense attention has been directed at *E*-field controlled 180° magnetization switching in FM films with the in-plane or perpendicular magnetic anisotropy.

4.1. In-plane 180° magnetization switching

In addition to the expected non-volatile 90° rotation of EA under *E*-fields, non-volatile in-plane 180° magnetization

reversal in Co/(001) PMN-PT with the aid of a small auxiliary magnetic field was also achieved at room temperature. As shown in Fig. 8(a), the magnetization first switches from the [010] (stage 1) to [-100] direction (stage 2) under the application of a +5 kV/cm pulse, and then switches to the opposite [0-10] direction (stage 3) under the application of a −5 kV/cm pulse without the assistance of magnetic fields. Then the +5 kV/cm pulse causes the magnetization to switch to the [-100] (stage 4) direction, and a subsequent −5 kV/cm pulse switches the magnetization to the [010] (stage 1) direction with the assistance of an auxiliary magnetic field pulse of 3 Oe. Thus, the 180° magnetization reversal process can be achieved using the described electric and magnetic pulse sequence.[64] However, in FM/AFM/PMN-PT(or PZN-PT) heterostructures, in-plane 180° magnetization switching could be realized using the exchange bias effect in FM/AFM structures instead of an external magnetic field.[65,66] For example, in CoFeB/IrMn/(011)PMN-PT heterostructures, the E-field induced converse ME coupling effect could change the ratio between the strain induced UMA field and the unidirectional exchange bias field. When the measured direction β, which is the angle of deviation of the [100] direction of PMN-PT, is in the middle of the dark gray region of the angular dependences of the remanent magnetization curves under different E-fields as shown in Fig. 8(b), magnetization reversal can be obtained at zero magnetic fields. Figure 8(c) shows the M–H loops under 8 kV/cm and 0 kV/cm with $\beta = 37°$. One can see that an obvious separation at the zero magnetic field appears, indicating that the E-field controlled in-plane 180° magnetization reversal is achieved under zero magnetic field by optimizing the anisotropy configuration in an exchange biased system.[66] The reversible E-field controlled magnetization reversal at zero magnetic fields in FM/AFM/FE heterostructures is greatly important for practical ultralow power consumption spintronic devices. Alternatively, Wang *et al.* proposed a simple and novel method to realize magnetization switching in nanomagnets with four-fold symmetric anisotropy. The flower-shaped nanomagnets deposited on an FE layer, and the E-field induced magnetoelastic axis cants an appropriate angle with respect to the EA of the nanomagnets. Using phase field simulations and thermodynamic analysis, in-plane 180° magnetization switching controlled by pure E-fields can be accomplished by two successive and deterministic 90° switching.[67]

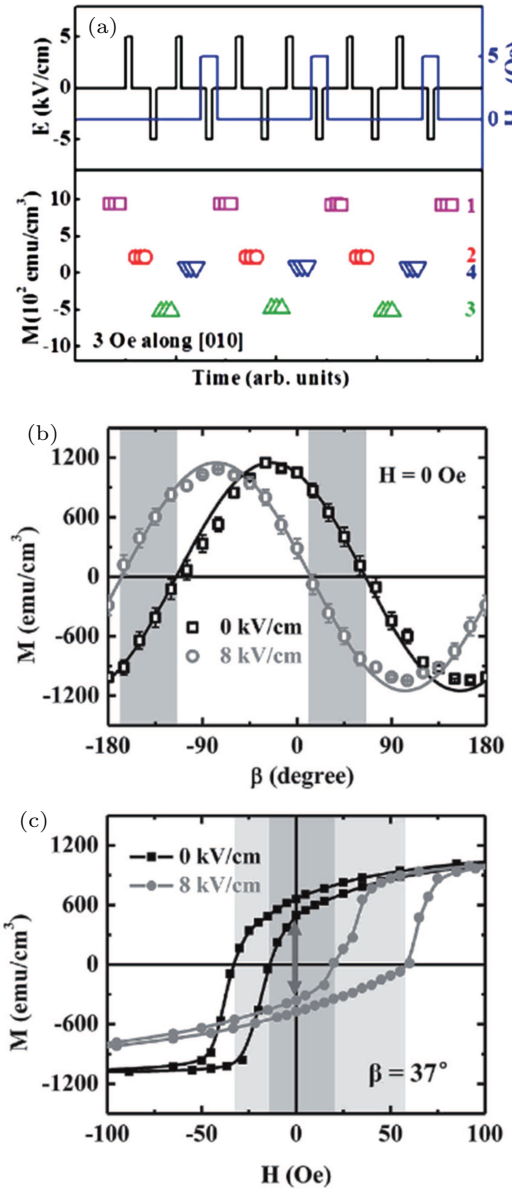


Fig. 8. (color online) (a) Pulsed electrical operation with H_{au} (top) and the resulting magnetization (bottom) measured in a magnetic field of 3 Oe along [010] (from Figs. 4(a) and 4(b) in Ref. [64]). (b) Angular dependence of M with and without an E-field at the zero magnetic field. (c) M–H loops at $\beta = 37°$ with the E-field of 0 and 8 kV/cm, respectively. (from Figs. 5(b) and 5(c) in Ref. [66]).

4.2. PMA modification and 180° perpendicular magnetization reversal

Compared with FM films with in-plane magnetic anisotropy, FM films with perpendicular magnetic anisotropy (PMA) have useful applications in STT-MARMs and SOT-MRAMs because they can effectively enhance the storage density.[68,69] It is accepted that PMA mainly originates from the interfacial magnetic anisotropy in ultrathin films, and the in-plane magnetic anisotropy results from the bulk magnetic anisotropy including the magnetocrystalline, random anisotropy or shape anisotropy. Therefore, the spin reorientation transition (SRT) is usually modified by changing the thickness of the films.[70–72] In $(Co/Pt)_3$/(011)PMN-PT heterostructures, both the interface and the bulk contributions to anisotropy coexist at a critical Co layer thickness range. Sun *et al.* first reported on E-field manipulation of the interface magnetic anisotropy and SRT of $(Co/Pt)_3$ multilayer at the critical thickness.[73] E-field modified variation of the first order volume anisotropy and interface anisotropy are 0.88% and −5.2%, respectively, whereas the E-field effect on the second-order volume anisotropy and interface anisotropy is very weak (Fig. 9(a)). This indicates that the E-field driven SRT is mainly

attributed to the strain controlled interface anisotropy. The results can be understood in terms of the E-field induced tensile strain which increases the distance between Pt and Co atoms. This, in turn, could reduce the hybridization between Pt 5d and Co 3d electrons, and weaken the PMA of $(Co/Pt)_3$/(011)PMN-PT. Meanwhile, Peng *et al.* demonstrated E-field controlled switching between the in-plane and out-of-plane magnetization in $(Co/Pt)_3$/(011) PMN-PT at room temperature.[74] The E-field controlled the strength of the PMA, and subsequently resulted in SRT in ultrathin films which are bound to accelerate the application of the low power ME devices.

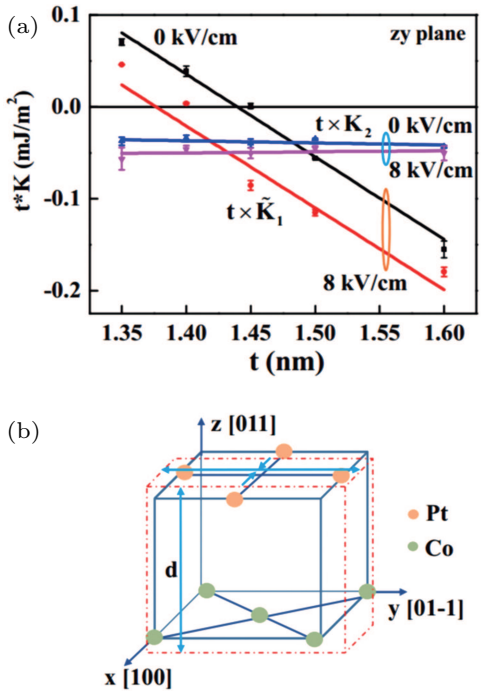


Fig. 9. (color online) (a) Plots of $t \times \tilde{K}_1$ vs. t ($t \times \tilde{K}_2$ vs. t) with and without an E-field and the corresponding linear fitting. (b) Schematic for strain-induced lattice changes at the Co/Pt interface (from Figs. 4(c) and 4(d) in Ref. [73]).

Recently, heavy metal/FM (HM/FM) bilayers with PMA received significant attention because they can utilize current induced SOT to realize magnetization switching.[12,75] Due to the strong SOC effect in HMs, their in-plane charge current can be converted to a pure spin current or interfacial spin accumulation by the spin Hall effect or Rashba effect, from the inversion asymmetry interface. The spin diffuses into the adjacent FM layer and switches the magnetization orientation through the SOT effect. In this process, a small in-plane assisted magnetic field is necessary to realize the 180° perpendicular magnetization reversal.[11,76] This is not convenient for practical applications. Thus, many investigations are focused on the realization of deterministic magnetization switching without any magnetic fields.[77–79] Cai *et al.* demonstrated deterministic magnetization switching in the symmetric Pt/Co/Ni/Co/Pt/(001) PMN-PT heterostructure combined with the E-field effect and the current effect.[80] As shown in the measurement schematic of Fig. 10(a), after the application of voltage values of +500 V (−500 V), a clockwise (anticlockwise) loop of the magnetization switching was observed (Figs. 10(b) and 10(c)). Meanwhile, after applying +500 V voltage, the reversible and non-volatile magnetization between up and down (180° magnetization reversal) can be modified by the in-plane current of −0.3 mA and +0.3 mA (Fig. 10(d)). Since the piezoelectric strain effect and interface Rashba effect are excluded, the E-field induced extra gradient spin density torque on the magnetization is the critical factor for the magnetization switching without external magnetic fields. The progress on deterministic 180° magnetization switching will be significant in the future design of spintronic and logic devices with low power consumption.

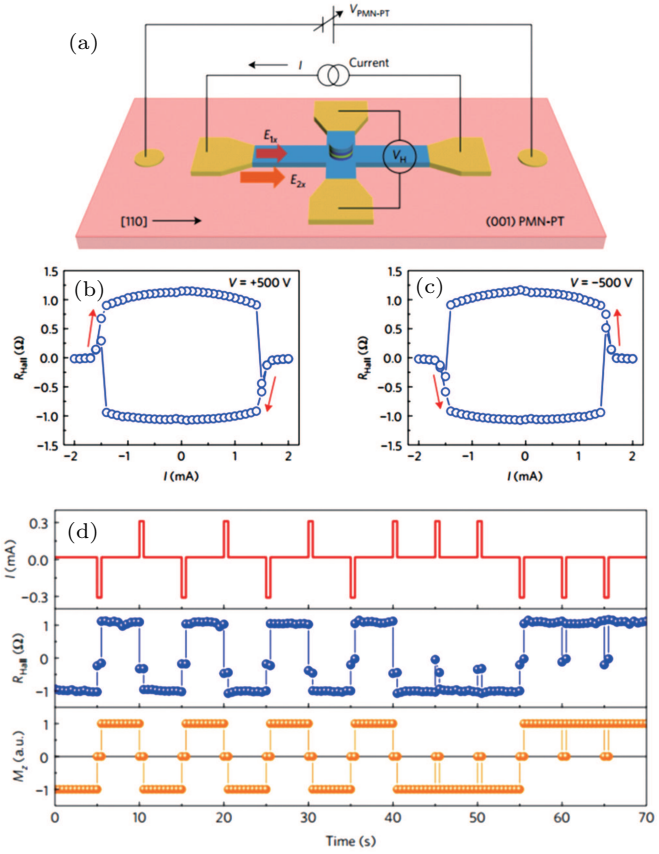


Fig. 10. (color online) (a) Schematic diagram of the measurement set-up. The voltage is applied to the PMN-PT substrates along the x-direction with a distance of 1 mm between the two electrodes. The applied voltage of VPMN-PT was removed during the current switching measurements. (b), (c) The current-induced magnetization switching after the polarization with the voltages of +500 V and −500 V on the PMN-PT substrate. (d) The deterministic magnetization switching by a series of current pulses applied to the device with 3-nm-thick bottom Pt layer. A small current I_M ($\sim$ 0.1 mA) was applied to measure the Hall resistance to distinguish the magnetization state (from Fig. 2 in Ref. [80]).

5. Conclusion and perspectives

In this review, we provided a summary of E-field controlled magnetization switching and magnetic anisotropy transition with an emphasis on the strain-mediated magnetism

in FM/FE heterostructures. By considering volatile to non-volatile magnetization switching, isotropic to UMA to CMA variations, and in-plane UMA to out-of-plane PMA materials, we discussed the developments of E-field controlled macro scale magnetism variation based on special experimental or theoretical results for electric field generated strain in FM/FE heterostructures. However, some outstanding issues still need to be solved, which range from understanding the fundamental physical mechanism of an operation to the realization of practical applications.

(I) Since materials like PMN-PT used by many research groups are nominally the same, the observed E-field controlled converse ME responses were multifarious. Hence, more attention should be paid to the repeatability and the stability of the experimental results, as well as the intrinsic physical mechanism of the electric field induced magnetization switching.

(II) E-field controlled magnetization switching paves the way to a new generation of spintronic devices. However, the existing difficulties need to be addressed with regards to integration and miniaturization for magnetic storage applications, such as MRAM combined with the GMR or TMR effect.

References

[1] Moodera J S, Kinder L R, Wong T M and Meservey R 1995 *Phys. Rev. Lett.* **74** 3273
[2] Wei H X, Qin Q H, Ma M, Sharif R and Han X F 2007 *J. Appl. Phys.* **101** 09B501
[3] Parkin S S P, Kaiser C, Panchula A, Rice P M, Hughes B, Samant M and Yang S H 2004 *Nat. Mater.* **3** 862
[4] Ikeda S, Hayakawa J, Ashizawa Y, Lee Y M, Miura K, Hasegawa H, Tsunoda M, Matsukura F and Ohno H 2008 *Appl. Phys. Lett.* **93** 082508
[5] Chappert C, Fert A and Dau F N V 2007 *Nat. Mater.* **6** 813
[6] Zhu J G 2008 *Proc. IEEE* **96** 1786
[7] Slonczewski J C 1996 *J. Magn. Magn. Mater.* **159** L1
[8] Berger L 1996 *Phys. Rev. B* **54** 9353
[9] Myers E B, Ralph D C, Katine J A, Louie R N and Buhrman R A 1999 *Science* **285** 867
[10] Miron I M, Gaudin G, Auffret S, Rodmacq B, Schuhl A, Pizzini S, Vogel J and Gambardella P 2010 *Nat. Mater.* **9** 230
[11] Liu L, Lee O J, Gudmundsen T J, Ralph D C and Buhrman R A 2012 *Phys. Rev. Lett.* **109** 096602
[12] Liu L, Pai C F, Li Y, Tseng H W, Ralph D C and Buhrman R A 2012 *Science* **336** 555
[13] https://www.everspin.com/files/everspin-releases-highest-density-mram-products-final-041216pdf
[14] Kim Y, Fong X, Kwon K W, Chen M C and Roy K 2015 *IEEE Trans. Electron. Devices* **62** 561
[15] Van d B A, Vermijs G, Solignac A, Koo J, Kohlhepp J T, Swagten H J and Koopmans B 2016 *Nat. Commun.* **7** 10854
[16] Lambert C H, Mangin S, Varaprasad B S, Takahashi Y K, Hehn M, Cinchetti M, Malinowski G, Hono K, Fainman Y, Aeschlimann M and Fullerton E E 2014 *Science* **345** 1337
[17] Cao J and Wu J 2011 *Sci. Eng. R* **71** 35
[18] Kharel P, Sudakar C, Dixit A, Harris A B, Naik R and Lawes G 2009 *Europhys. Lett.* **86** 17007
[19] Wu S M, Cybart S A, Yu P, Rossell M D, Zhang J X, Ramesh R and Dynes R C 2010 *Nat. Mater.* **9** 756
[20] Ohno H, Chiba D, Matsukura F, Omiya T, Abe E, Dietl T, Ohno Y and Ohtani K 2000 *Nature* **408** 944
[21] Bauer U, Yao L, Tan A J, Agrawal P, Emori S, Tuller H L, van Dijken S and Beach G S D 2015 *Nat. Mater.* **14** 174
[22] Ramesh R and Spaldin N A 2007 *Nat. Mater.* **6** 21
[23] Lei N, Devolder T, Agnus G, Aubert P, Daniel L, Kim J V, Weisheng Z, Trypiniotis, T, Cowburn R P, Chappert C, Ravelosona D and Lecoeur P 2013 *Nat. Commun.* **4** 1378
[24] Rushforth A W, Ranieri E D, Zemen J, Wunderlich J, Edmonds K W, King C S, Ahmad E, Campion R P, Foxon C T, Gallagher B L, Vyborny K, Kucera J and Jungwirth T 2008 *Phys. Rev. B* **78** 085314
[25] Li Y, Luo W, Zhu L, Zhao J and Wang K Y 2015 *J. Magn. Magn. Mater.* **375** 148
[26] Khomskii D I 2009 *Physics* **2** 20
[27] Ma J, Hu J, Li Z and Nan C W 2011 *Adv. Mater.* **23** 1061
[28] Lu C J, Li P, Wen Y M, Yang A C, Yang C, Wang D C, He W and Zhang J T 2014 *Chin. Phys. B* **23** 117503
[29] Wang K F, Liu J M and Ren Z F 2009 *Adv. Phys.* **58** 321
[30] Sen P, Dey A, Mukhopadhyay A K, Bandyopadhyay S K and Himanshu A K 2012 *Ceram. Int.* **38** 1347
[31] Song C, Cui B, Li F, Zhou X and Pan F 2017 *Prog. Mater. Sci.* **87** 33
[32] Sahoo S, Polisetty S, Duan C G, Jaswal S S, Tsymbal E Y and Binek C 2007 *Phys. Rev. B* **76** 092108
[33] Bar-Chaim N, Brunstein M, Grünberg J and Seidman A 1974 *J. Appl. Phys.* **45** 2398
[34] Li Z, Xu Z, Yao X and Cheng Z Y 2008 *J. Appl. Phys.* **104** 024112
[35] Liu M, Obi O, Cai Z, Lou J, Yang G, Ziemer K S and Sun N X 2010 *J. Appl. Phys.* **107** 073916
[36] Vaz C A F 2012 *J. Phys.: Condens. Matter* **24** 333201
[37] Song C, Cui B, Peng J J, Mao H J and Pan F 2016 *Chin. Phys. B* **25** 067502
[38] He H, Zhao J, Luo Z, Yang Y, Xu H, Hong B, Wang L, Wang R and Gao C 2016 *Chin. Phys. Lett.* **33** 67502
[39] Tiercelin N, Dusch Y, Klimov A, Giordano S, Preobrazhensky V and Pernod P 2011 *Appl. Phys. Lett.* **99** 192507
[40] Liu M, Li S, Zhou Z, Beguhn S, Lou J, Xu F, Lu T J and Sun N X 2012 *J. Appl. Phys.* **112** 063917
[41] Yang L, Zhao Y, Zhang S, Li P, Gao Y, Yang Y, Huang H, Miao P, Liu Y, Chen A, Nan C W and Gao C 2015 *Sci. Rep.* **4** 4591
[42] Yang J J, Zhao Y G, Tian H F, Luo L B Zhang H Y, He Y J and Luo H S 2009 *Appl. Phys. Lett.* **94** 212504
[43] Thiele C, Ouml K, rr, Bilani O, Ouml J and Schultz D 2007 *Phys. Rev. B* **75** 054408
[44] Zhang S, Zhao Y, Xia X, Wu Y, Rizwan S, Yang L, Li P, Wang J, Zhu M, Zhang H, Jin X and Han X 2015 *Sci. Rep.* **4** 3727
[45] Xi L, Guo X B, Wang Z, Li Y, Yao Y L, Zuo Y L and Xue D S 2013 *Appl. Phys. Express* **6** 015804
[46] Tiercelin N, Dusch Y, Klimov A, Giordano S, Preobrazhensky V and Pernod P 2011 *Appl. Phys. Lett.* **99** 192507
[47] Cui B S, Guo X B, Wu K, Li D, Zuo Y L and Xi L 2016 *J. Phys. D: Appl. Phys.* **49** 085002
[48] Chen A T and Zhao Y G 2016 *APL Mater.* **4** 032303
[49] Liu M, Nan T, Hu J M, Zhao S S, Zhou Z, Wang C Y, Jiang Z D, Ren W, Ye Z G, Chen L Q and Sun N X 2016 *NPG Asia Mater.* **8** e316
[50] Wu T, Bur A, Zhao P, Mohanchandra K P, Wong K, Wang K L, Lynch C S and Carman G P 2011 *Appl. Phys. Lett.* **98** 012504
[51] Wu T, Zhao P, Bao M, Bur A, Hockel J L, Wong K, Mohanchandra K P, Lynch C S and Carman G P 2011 *J. Appl. Phys.* **109** 124101
[52] Han X, Xi L, Li Y, Guo X, Li D, Wang Z, Zuo Y and Xue D 2014 *Appl. Phys. Lett.* **105** 122402
[53] Liu M, Howe B M, Grazulis L, Mahalingam K, Nan T, Sun N X and Brown G J 2013 *Adv. Mater.* **25** 4886
[54] Zhang S, Zhao Y G, Li P S, *et al.* 2012 *Phys. Rev. Lett.* **108** 137203
[55] Liu M, Obi O, Lou J, Chen Y, Cai Z, Stoute S, Espanol M, Lew M, Situ X, Ziemer K S, Harris V G and Sun N X 2009 *Adv. Funct. Mater.* **19** 1826
[56] Chen Y J, Gao J, Fitchorov T, Cai Z, Ziemer K S, Vittoria C and Harris V G 2009 *Appl. Phys. Lett.* **94** 082504
[57] Guo X B, Wu K, Cui B S, Li D, Yun J J, Zuo Y L, Zuo H P, Wang T and Xi L 2016 *J. Phys. D: Appl. Phys.* **49** 055005
[58] Guo X, Zuo Y, Li D, Cui B, Wu K, Yun J, Wang T and Xi L 2016 *Appl. Phys. Lett.* **108** 042403
[59] Parkes D E, Cavill S A, Hindmarch A T and Wadley P 2012 *Appl. Phys. Lett.* **101** 072402
[60] Guo X, Han X, Zuo Y, Zhang J, Li D, Cui B, Wu K, Yun J, Wang T, Peng Y and Xi L 2016 *Appl. Phys. Lett.* **108** 152401
[61] Zhang B, Meng K K, Yang M Y, Edmonds K, Zhang H, Cai K M, Sheng Y, Zhang N, Ji Y, Zhao J H, Zheng H Z and Wang K Y 2016 *Sci. Rep.* **6** 28458

[62] Zhang N, Zhang B, Yang M Y, Cai K M, Sheng Y, Li Y C, Deng Y C and Wang K Y 2017 *Acta Phys. Sin.* **66** 027501 (in Chinese)
[63] Guo X, Cui B, Guan C, Li D, Wu K, Yun J, Wang T, Peng Y, Zuo Y and Xi L 2017 *J. Phys. D: Appl. Phys.* **50** 335001
[64] Yang S W, Peng R C, Jiang T, Liu Y K, Feng L, Wang J J, Chen L Q, Li X G and Nan C W 2014 *Adv. Mater.* **26** 7091
[65] Liu M, Lou J, Li S and Sun N X 2011 *Adv. Funct. Mater.* **21** 2593
[66] Chen A, Zhao Y, Li P, Zhang X, Peng R, Huang H, Zou L, Zheng X, Zhang S, Miao P, Lu Y, Cai J and Nan C W 2016 *Adv. Mater.* **28** 363
[67] Wang J J, Hu J M, Ma J, Zhang J X, Chen L Q and Nan C W 2015 *Sci. Rep.* **4** 7507
[68] Shaw J M, Nembach H T and Silva T J 2013 *Phys. Rev. B* **87** 054416
[69] Hu J M, Yang T, Wang J, Huang H, Zhang J, Chen L Q and Nan C W 2015 *Nano Lett.* **15** 616
[70] Oepen H P, Speckmann M, Millev Y and Kirschner J 1997 *Phys. Rev. B* **55** 2752
[71] Farle M 1998 *Rep. Prog. Phys.* **61** 755
[72] Millev Y and Kirschner J 1996 *Phys. Rev. B* **54** 4137
[73] Sun Y, Ba Y, Chen A, *et al.* 2017 *ACS Appl. Mater. Interfaces* **9** 10855
[74] Peng B, Zhou Z, Nan T, Dong G, Feng M, Yang Q, Wang X, Zhao S, Xian D, Jiang Z D, Ren W, Ye Z G, Sun N X and Liu M 2017 *ACS Nano* **11** 4337
[75] Miron I M, Garello K, Gaudin G, Zermatten P J, Costache M V, Auffret S, Bandiera S, Rodmacq B, Schuhl A and Gambardella P 2011 *Nature* **476** 189
[76] Liu L, Lee O J, Gudmundsen T J, Ralph D C and Buhrman R A 2012 *Phys. Rev. Lett.* **109** 096602
[77] Yu G, Upadhyaya P, Fan Y, Alzate J G, Jiang W, Wong K L, Takei S, Bender S A, Chang L T, Jiang Y, Lang M, Tang J, Wang Y, Tserkovnyak Y, Amiri P and Wang K L 2014 *Nat. Nanotechnol.* **9** 548
[78] Pai C F, Mann M, Tan A J and Beach G S D 2016 *Phys. Rev. B* **93** 144409
[79] Lau Y C, Betto D, Rode K, Coey J M and Stamenov P 2016 *Nat. Nanotechnol.* **11** 758
[80] Cai K, Yang M, Ju H, Wang S, Ji Y, Li B, Edmonds K W, Sheng Y, Zhang B, Zhang N, Liu S, Zheng H and Wang K 2017 *Nat. Mater.* **16** 712